Chapter 10

3-D FOCUSING INVERSION OF CSAMT DATA

Oleg Portniaguine and Michael S. Zhdanov

University of Utah, Salt Lake City, UT 84112, USA

Abstract: We present a method for the solution of 3-D controlled source magnetotelluric (CSAMT) inverse problems. The inverse problem is formulated as the minimization of a Tikhonov parametric functional with a focusing stabilizer. Observed CSAMT apparent resistivities are converted to log-anomalous apparent resistivities, which are linearly connected to anomalous currents via the integral equation. We apply the Born iterative method to solve this integral equation, using a focusing regularized inversion. The focusing is based on a specially selected stabilizing functional which minimizes the area where strong model parameters variations and discontinuities occur. The method is illustrated using examples of 3-D inversion of model CSAMT data, and with a real data example.

1. INTRODUCTION

This paper deals with three particular aspects of the CSAMT inverse problem. The first is use of apparent resistivity data in the inversion, which is solved by using the concept of *log-anomalous apparent resistivity*. The second aspect is nonlinearity of the inverse problem, for the solution of which we apply the Born iterative method (Chew, 1990). The third is the non-uniqueness of the solution, which is addressed by using Tikhonov's regularization theory.

Traditional geophysical inversion methods are often based on the Tikhonov regularization theory (Tikhonov and Arsenin, 1977; Zhdanov, 1993) which provides a stable solution of the inverse problem. This goal is reached, as a rule, by introducing a maximum smoothness stabilizing functional. The obtained solution provides a smooth image of real structures that sometimes looks geologically unrealistic. Recently a new approach to the reconstruction of noisy images has been developed (Rudin et al., 1992; Vogel and Oman, 1998). It is based on a total variation stabilizing functional which requires that the distribution of the model parameters be of bounded variation. This requirement is weaker than one of maximum smoothness because it can be applied to discontinuous functions. However, it still decreases the bounds of the model parameters' variations and therefore distort the image. In papers by Portniaguine and Zhdanov (1998, 1999) we introduced stabilizing functionals, which generate more 'focused' images than conventional methods. We call this approach *focusing of inversion images*. In the present paper we apply this new method to the 3-D CSAMT inversion.

The CSAMT method measures complex impedances, which are often converted to apparent resistivity and phase. For 3-D inversion, the apparent resistivities have to be connected to fields. We solve this problem by converting data to *log-anomalous apparent resistivities*, which are linearly connected to anomalous fields. Such conversion has certain advantages, as opposed to using anomalous fields directly. Often, only the value of apparent resistivity is measured. This makes calculation of the anomalous fields difficult, because recomputing apparent resistivity into anomalous fields requires knowledge of phases. Log-anomalous apparent resistivity can be easily computed without knowing the phase. Another aspect is that the measurements at different frequencies should be properly weighted to invert them together. Conversion to log-anomalous apparent resistivity makes the measurements dimensionless, which provides natural weighting to the fields at different frequencies. These advantages apply to inverse problems both for layered media (finding the background field) and for the subsequent 3-D inversion.

The electromagnetic (EM) inverse problem is nonlinear. For ease of numerical solution, it is often converted to a series of linear problems. One common technique is the Born iterative method (Chew, 1990). This method is based on the fact that the EM inverse problem is actually a bi-linear problem, a special case of a general nonlinear problem. Since the problem is linear to anomalous currents, and the currents are the product of the total electric field and anomalous conductivity, the inverse problem becomes linear with respect to conductivity if the total fields are fixed. The total electric fields, in turn, are connected to anomalous conductivity via the corresponding integral equation (IE). Using these properties, we construct an iterative process whereby the linear inverse problem is solved first for anomalous currents, assuming the total electric fields are fixed. Second, the values of the total fields are updated using the found values of anomalous currents. These new values of the total fields are used in the next iteration of the inverse problem. Convergence of the process is assured by using a modified Green's tensor operator (Zhdanov and Fang, 1997).

Combined with the focusing inversion method, such a strategy allows us to avoid solving the full IE for the whole inversion domain. On the first iteration, the linear inverse problem produces compact bodies, and the total electric field needs to be found only inside the compact domains. The IE for such domains is much smaller than the IE for the whole domain and can be easily solved.

Our discussion is illustrated by applications of the method to synthetic models and real CSAMT data, collected in Hamlin Valley, Nevada, for oil exploration.

2. THE METHOD OF INTEGRAL EQUATIONS

The IE method is a powerful tool for EM modeling and inversion. The basic principles of constructing integral equations in 3-D cases were outlined by Weidelt (1975) and Hohmann (1975). A comprehensive implementation of the IE methods was realized by Xiong (1992) in the SYSEM code. Also, several IE-based approximate methods have been developed recently. These are localized nonlinear approximation (Habashi et al., 1993), quasi-linear approximation (Zhdanov and Fang, 1996a,b), quasi-linear series (Zhdanov and Fang, 1997), and quasi-analytic approximation (Zhdanov et al., 2000).

The main idea of the IE method is the following. The forward EM problem consists of finding the electric and magnetic fields at receivers for a given source and with known distribution of electrical conductivity (Zhdanov and Keller, 1994). We assume that the magnetic permeability μ is constant everywhere and is equal to that of free space $\mu = 4\pi \times 10^{-7}$ H/m. Let us represent a 3-D distribution of conductivity σ as the sum of background (normal) conductivity σ_b and anomalous conductivity $\Delta\sigma$, which is nonzero only within the local domain D. This model is excited by a harmonic source of circular frequency ω.

The vectors of total electric $\mathbf{E}$ and magnetic $\mathbf{H}$ fields in this model can be presented as the sum of background (normal) and anomalous (scattered) fields:

$$\mathbf{E} = \mathbf{E}^b + \mathbf{E}^a, \quad \mathbf{H} = \mathbf{H}^b + \mathbf{H}^a. \tag{10.1}$$

The background field $\mathbf{E}^b$ is a field generated by the given sources in the background model σ_b, and the anomalous $\mathbf{E}^a$ field is caused by the presence of anomalous conductivity $\Delta\sigma$.

The anomalous field is presented as an integral over the excess currents in the inhomogeneous domain D:

$$\mathbf{E}^a(\mathbf{r}_j) = \iiint_D \widehat{\mathbf{G}}_E(\mathbf{r}_j \mid \mathbf{r}) \cdot \mathbf{j}^a(\mathbf{r})\, dv, \tag{10.2}$$

$$\mathbf{H}^a(\mathbf{r}_j) = \iiint_D \widehat{\mathbf{G}}_H(\mathbf{r}_j \mid \mathbf{r}) \cdot \mathbf{j}^a(\mathbf{r})\, dv, \tag{10.3}$$

where $\widehat{\mathbf{G}}_\mathbf{E}(\mathbf{r}_j \mid \mathbf{r})$ and $\widehat{\mathbf{G}}_\mathbf{H}(\mathbf{r}_j \mid \mathbf{r})$ are the electric and magnetic Green's tensors defined for an unbounded conductive medium with a background conductivity σ_b. Excess (anomalous) current density $\mathbf{j}^a(\mathbf{r})$ at point $\mathbf{r}$ is determined by the equation

$$\mathbf{j}^a(\mathbf{r}) = \Delta\sigma(\mathbf{r})\left(\mathbf{E}^b(\mathbf{r}) + \mathbf{E}^a(\mathbf{r})\right) = \Delta\sigma(\mathbf{r})\mathbf{E}(\mathbf{r}). \tag{10.4}$$

Expression (10.2) becomes the IE with respect to anomalous electric field $\mathbf{E}^a(\mathbf{r})$, if point $\mathbf{r}_j$ is inside D. Solution of this equation yields an anomalous electric field inside domain D. After that, anomalous magnetic fields everywhere and anomalous electric fields outside domain D can be found using Equations (10.2) and (10.3). The background fields are assumed to be known everywhere.

In turn, the anomalous field is a linear combination of anomalous currents $\Delta\sigma(r)\mathbf{E}(\mathbf{r})$:

$$\mathbf{E}^a(\mathbf{r}_j) = \iiint_D \widehat{\mathbf{G}}_E(\mathbf{r}_j \mid \mathbf{r}) \cdot \Delta\sigma(r)\mathbf{E}(\mathbf{r})\, dv, \tag{10.5}$$

$$\mathbf{H}^a(\mathbf{r}_j) = \iiint_D \widehat{\mathbf{G}}_H(\mathbf{r}_j \mid \mathbf{r}) \cdot \Delta\sigma(\mathbf{r})\mathbf{E}(\mathbf{r})\, dv. \tag{10.6}$$

We use discrete analogs of the continuous Equations (10.5), (10.6):

$$\mathbf{E}_a = \widehat{\mathbf{G}}_e \widehat{\mathbf{S}}\mathbf{e}_t, \tag{10.7}$$

$$\mathbf{H}_a = \widehat{\mathbf{G}}_h \widehat{\mathbf{S}} \mathbf{e}_t, \tag{10.8}$$

where discrete vector $\mathbf{e}_t$ contains three components of the total electric fields inside the anomalous domain, and the vectors $\mathbf{E}_a$ and $\mathbf{H}_a$ represent the anomalous fields at the receivers. The anomalous conductivity is stored in a sparse diagonal matrix $\widehat{\mathbf{S}}$. Matrices $\widehat{\mathbf{G}}_e$, $\widehat{\mathbf{G}}_h$ represent the values of corresponding Green's tensors.

If point $\mathbf{r}_j$ is inside the anomalous domain D, Expression (10.7) becomes an integral equation with respect to the electric field:

$$\mathbf{e}_a = \widehat{\mathbf{G}}\widehat{\mathbf{S}}\mathbf{e}_t, \tag{10.9}$$

where $\mathbf{e}_a$ is a vector of an anomalous field, and $\widehat{\mathbf{G}}$ is a matrix of the corresponding Green's tensor inside the domain D. Equation (10.9) establishes a connection between the electric field inside the anomalous domain and the anomalous conductivity. Using

$$\mathbf{e}_t = \mathbf{e}_a + \mathbf{e}_n, \tag{10.10}$$

where $\mathbf{e}_n$ is a vector of normal electric field inside the domain, Equation (10.9) becomes

$$\mathbf{e}_a = \widehat{\mathbf{G}}\widehat{\mathbf{S}}(\mathbf{e}_a + \mathbf{e}_n). \tag{10.11}$$

or

$$\mathbf{e}_t = \widehat{\mathbf{G}}\widehat{\mathbf{S}}\mathbf{e}_t + \mathbf{e}_n. \tag{10.12}$$

The solution to (10.12) can be written in matrix notation:

$$\mathbf{e}_t = (\widehat{\mathbf{I}} - \widehat{\mathbf{G}}\widehat{\mathbf{S}})^{-1}\mathbf{e}_n. \tag{10.13}$$

3. THE CSAMT FORWARD PROBLEM

The scalar CSAMT method produces values of a complex apparent resistivity ρ (Tikhonov, 1950; Cagniard, 1953), which is computed according to

$$\rho = \frac{1}{cf}\left(\frac{E_y}{H_x}\right)^2, \quad c = 2\pi\mu_0, \tag{10.14}$$

where f is frequency, μ_0 is the free space magnetic permeability, E_y is the y-component of an electric field, and H_x is the x-component of a magnetic field. We assume that measurement profiles are parallel to the y axis.

In general, apparent resistivity is a nonlinear function of electric and magnetic fields. It is possible, however, to derive a convenient simplification of the apparent resistivity formula which makes these dependencies linear. Below, we demonstrate that the logarithm of apparent resistivity is linearly connected to the anomalous fields.

We represent the field components as the sum of normal (denoted with subscript 'n') and anomalous parts (denoted by subscript 'a'):

$$E_y = E_n + E_a, \quad H_x = H_n + H_a. \tag{10.15}$$

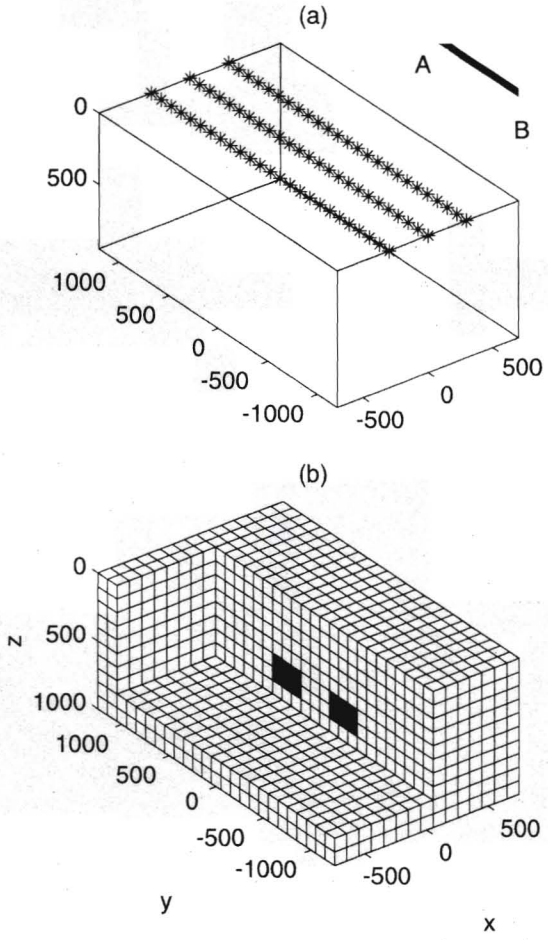

Figure 1. Synthetic EM model: (a) observation system, (b) true model.

Taking the log of Equation (10.14) and using Formula (10.15), we obtain

$$\ln(\rho) = \ln\left(\frac{1}{cf}\left(\frac{E_n + E_a}{H_n + H_a}\right)^2\right) = 2\ln(E_n + E_a) - 2\ln(H_n + H_a) - \ln(cf),$$

$$\ln(\rho) = 2\ln(1 + E_a/E_n) - 2\ln(1 + H_a/H_n) + 2\ln(E_n/H_n) - \ln(cf). \tag{10.16}$$

Provided that the anomalous field is much smaller than the normal field, the log of apparent resistivity can be easily linearized, using

$$\ln(1 + \Delta x) \approx \Delta x. \tag{10.17}$$

A *normal apparent resistivity* ρ_n can be introduced to obtain

$$\ln(\rho_n) = 2\ln(E_n/H_n) - \ln(cf) = \ln\left(\frac{1}{cf}\left(\frac{E_n}{H_n}\right)^2\right). \tag{10.18}$$

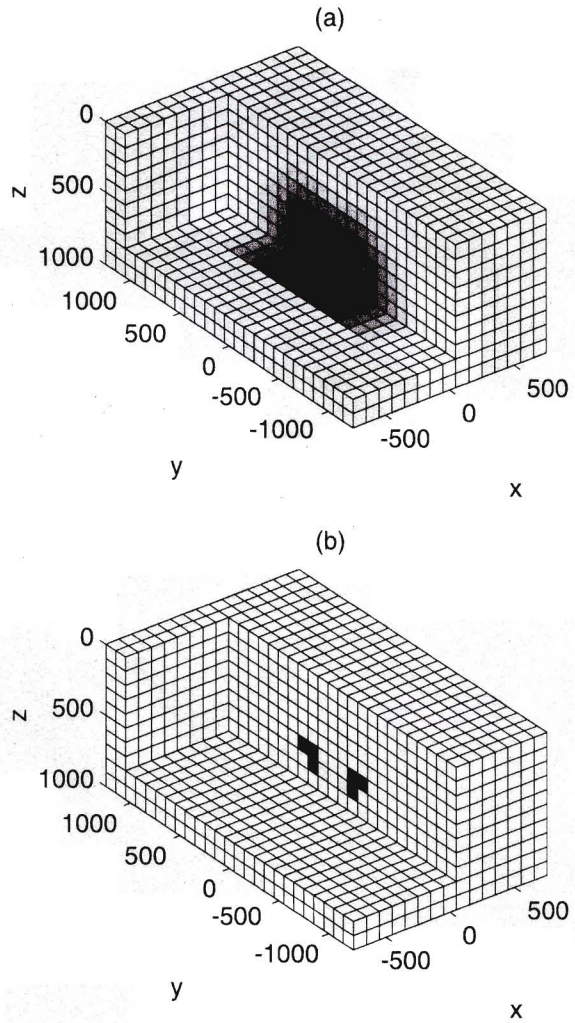

Figure 2. (a) 3-D resistivity model resulting from smooth inversion, 1.5% misfit. (b) Result of focusing inversion with 1.5% misfit.

Combining (10.16), (10.17) and (10.18), we have

$$\ln(\rho) = 2(E_a/E_n - H_a/H_n) + \ln(\rho_n). \tag{10.19}$$

Now we introduce *log-anomalous apparent resistivity* $\ln(\rho_a)$ as the difference between the logs of observed (total) and normal apparent resistivity:

$$\ln(\rho_a) = \ln(\rho) - \ln(\rho_n) = 2(E_a/E_n - H_a/H_n). \tag{10.20}$$

Note that the frequency term $\ln(1/cf)$ in (10.16) cancels. The quantities in (10.20) are dimensionless. Thus, expression (10.20) for different frequencies can be used together in the inversion without additional weighting. If we measure only the absolute value

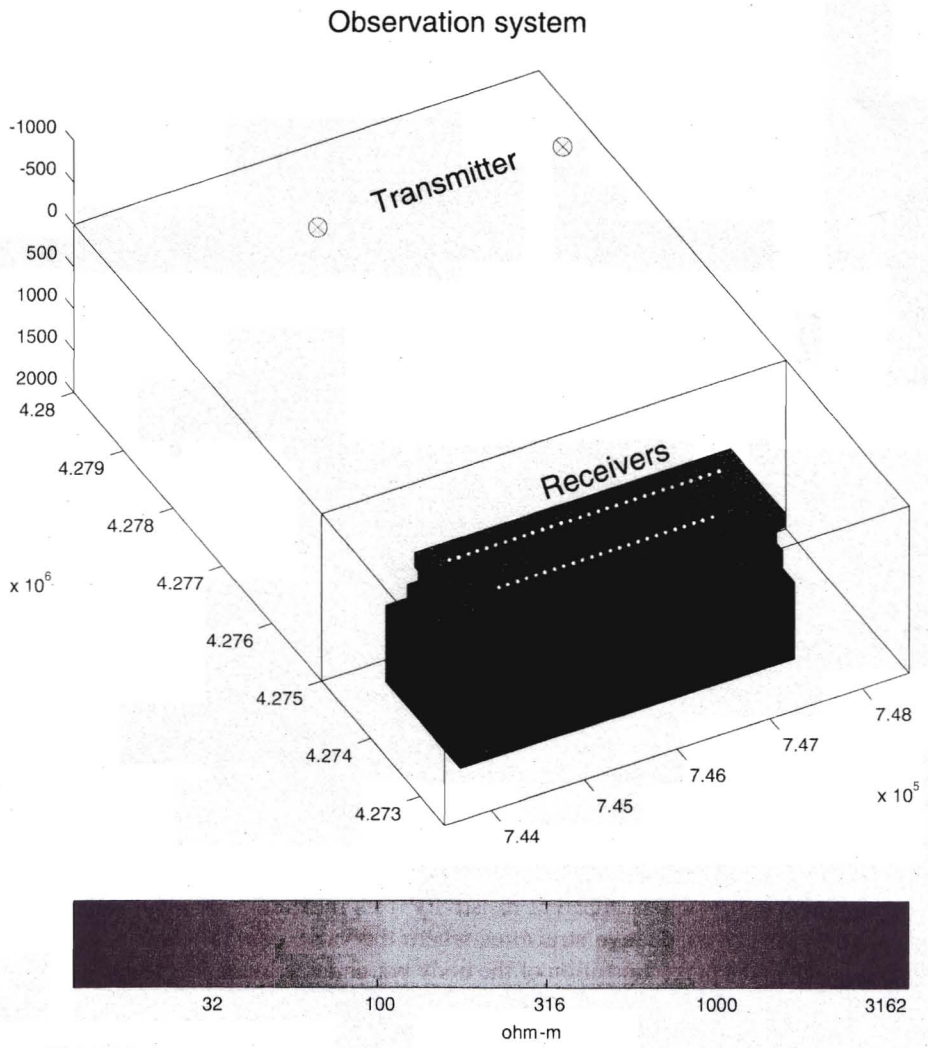

Figure 3. Background model with a resistive layer. The lower half-space is filled with rectangular cells. The size of the cells increases with depth. Stars denote the receiver location. Circles denote the location of the transmitter poles.

of apparent resistivity, but not phase, all we need to use is the real part of logarithmic Equation (10.20):

$$\ln|\rho_a| = 2\,\mathrm{Real}(E_a/E_n - H_a/H_n). \tag{10.21}$$

Note also that log-anomalous apparent resistivity is an approximation. Experiments with synthetic and real data show that the maximum of log-anomalous apparent resistivity is on the order of 0.2. For this value, linearization (10.17) holds with an accuracy of 0.01. The estimated noise in the 3-D inverse problem with respect to

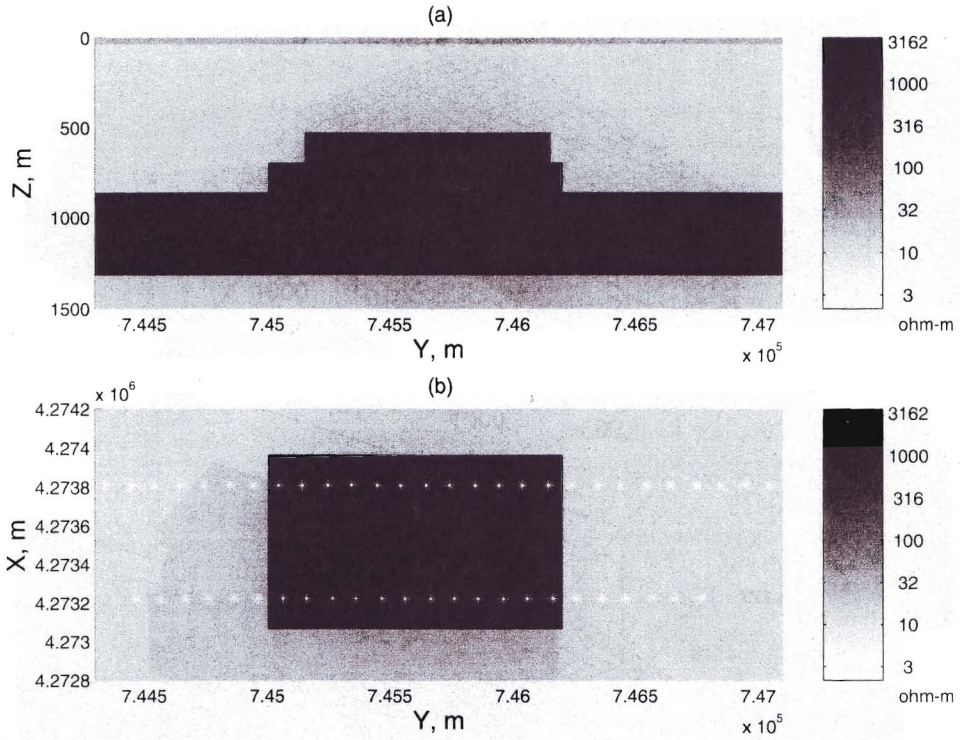

Figure 4. Model with the anticline on top of the resistive layer. (a) Cross-section. (b) Plan view; the slice is taken at 800 m depth. Stars denote the receiver locations.

log-anomalous apparent resistivity is also on the order of 0.01. Thus, we can safely use the notion of log-anomalous apparent resistivity if its maximum value is less than 0.2. For cases with very conductive structures where the value can be more than that, the algorithm shows the correct position of the body but underestimates the conductivity.

4. FORMULATION OF THE INVERSE PROBLEM

The inversion process consists of two major steps. First, we estimate normal apparent resistivity by fitting the log of observed apparent resistivity $\ln(\rho)$ for all stations *and all frequencies* with the log of apparent resistivity derived from a layered model $\ln(\rho_n)$. The residual of fitting is associated with log-anomalous apparent resistivity. As we can see from (10.20), log-anomalous apparent resistivity $\ln(\rho_a)$ is a linear combination of anomalous fields. Further, we represent anomalous field as a linear combination of responses from individual cells and solve the 3-D inverse problem using the method of focusing inversion.

We introduce a vector of the data $\mathbf{d}$, which combines the values of log-anomalous apparent resistivity at the receivers, for all frequencies. According to (10.20), it is

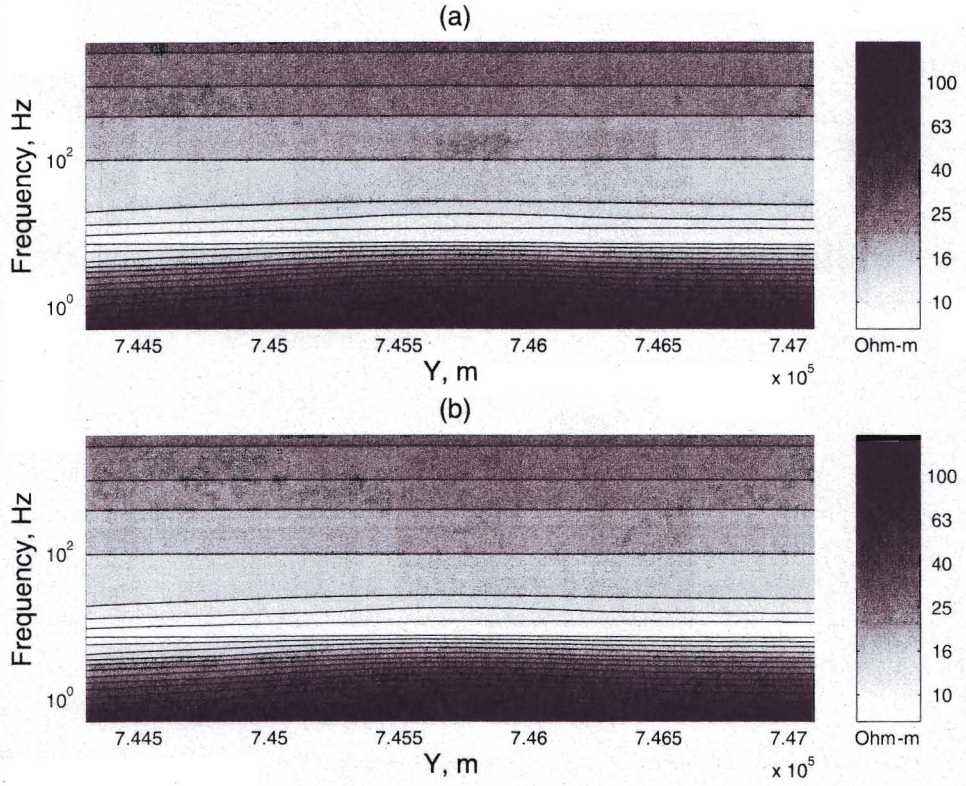

Figure 5. Data for the model shown in Figure 4. (a) Original log-anomalous apparent resistivity for the first profile. (b) Log-anomalous apparent resistivity predicted from the inversion.

a linear combination of anomalous fields, with normal fields as weights. In matrix notations, Formula (10.20) is cast as follows:

$$\mathbf{d} = 2(\mathrm{diag}(\mathbf{E}_\mathrm{n})^{-1}\mathbf{E}_\mathrm{a} - \mathrm{diag}(\mathbf{H}_\mathrm{n})^{-1}\mathbf{H}_\mathrm{a}), \tag{10.22}$$

where $\mathrm{diag}(\mathbf{E}_\mathrm{n})^{-1}$ and $\mathrm{diag}(\mathbf{H}_\mathrm{n})^{-1}$ are sparse matrices containing the inverse normal fields on the main diagonal.

Integral Equations (10.7) and (10.8) connect the anomalous fields at the receivers to anomalous currents $\widehat{\mathbf{S}}\mathbf{e}_\mathrm{t}$ inside the domain. We introduce sensitivity to the currents, matrix $\widehat{\mathbf{G}}_j$, as a linear combination of matrices $\widehat{\mathbf{G}}_e$ and $\widehat{\mathbf{G}}_h$:

$$\widehat{\mathbf{G}}_j = 2\,\mathrm{diag}(\mathbf{E}_\mathrm{n})^{-1}\widehat{\mathbf{G}}_e - 2\,\mathrm{diag}(\mathbf{H}_\mathrm{n})^{-1}\widehat{\mathbf{G}}_h. \tag{10.23}$$

Using (10.22) and (10.23), we convert Equations (10.7) and (10.8) into a single equation:

$$\mathbf{d} = \widehat{\mathbf{G}}_j\widehat{\mathbf{S}}\mathbf{e}_\mathrm{t}. \tag{10.24}$$

We formulate the inverse problem with respect to scaled conductivity $\mathbf{m}$, which is connected to anomalous conductivity via a matrix of expected conductivities $\widehat{\mathbf{S}}_e$ (constraints). The anomalous conductivity is a product of inversion parameter $\mathbf{m}$,

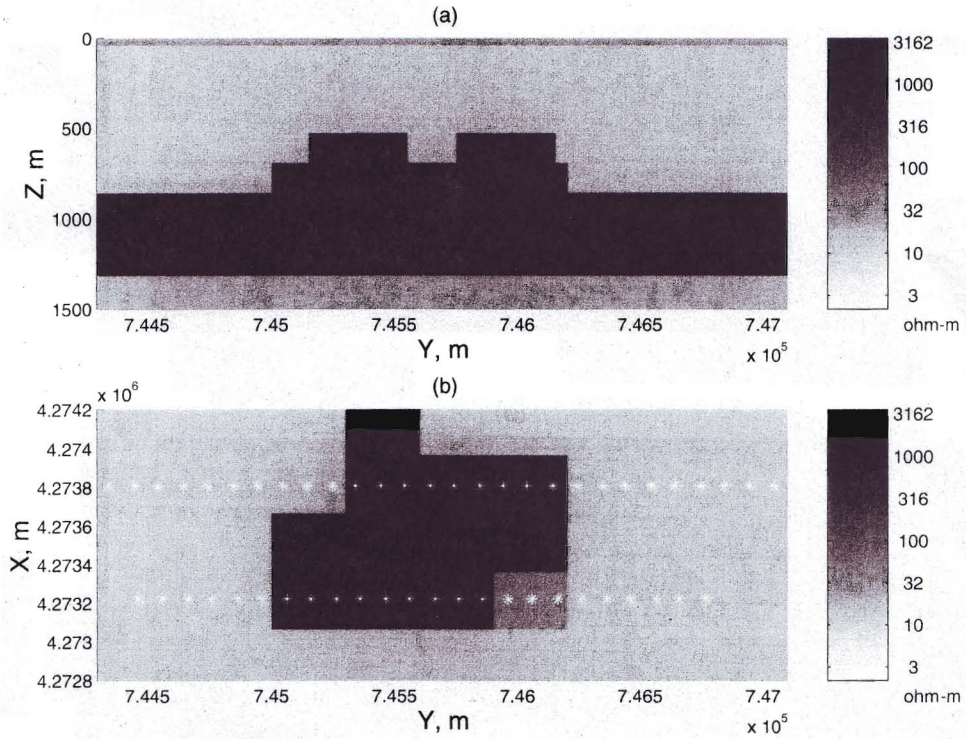

Figure 6. Result of inversion for the body atop the resistive layer. (a) Plan view. (b) Cross-section.

changing from -1 to 1, and the value of constraint, which is stored in the corresponding diagonal of matrix $\widehat{\mathbf{S}}_e$. The following relationships hold:

$$\widehat{\mathbf{S}} = \mathrm{diag}(\widehat{\mathbf{S}}_e \mathbf{m}), \tag{10.25}$$

$$\mathbf{S}\mathbf{e}_\mathrm{t} = \mathrm{diag}(\mathbf{e}_\mathrm{t})\widehat{\mathbf{S}}_e \mathbf{m} \tag{10.26}$$

Using (10.26) and (10.24), we establish the equation of the forward problem:

$$\mathbf{d} = \widehat{\mathbf{G}}_j \,\mathrm{diag}(\mathbf{e}_\mathrm{t})\widehat{\mathbf{S}}_e \mathbf{m}. \tag{10.27}$$

Or, expressing $\mathbf{e}_\mathrm{t}$ via (10.13), we may rewrite Equation (10.27) as

$$\mathbf{d} = \widehat{\mathbf{G}}_j \,\mathrm{diag}((\widehat{\mathbf{I}} - \widehat{\mathbf{G}}\,\mathrm{diag}(\widehat{\mathbf{S}}_e \mathbf{m}))^{-1}\mathbf{e}_\mathrm{n})\widehat{\mathbf{S}}_e \mathbf{m}. \tag{10.28}$$

Our goal is to find the parameters $\mathbf{m}$ given the data $\mathbf{d}$, that is to solve the inverse problem. Since this inverse problem is ill-posed, we use the Tikhonov regularization method to solve it. We minimize the Tikhonov parametric functional with a minimum support focusing stabilizer (Portniaguine and Zhdanov, 1999):

$$\|\mathbf{d} - \widehat{\mathbf{G}}_\mathbf{j}\,\mathrm{diag}((\widehat{\mathbf{I}} - \widehat{\mathbf{G}}\,\mathrm{diag}(\widehat{\mathbf{S}}_\mathbf{e}\mathbf{m}))^{-1}\mathbf{e}_\mathbf{n})\widehat{\mathbf{S}}_\mathbf{e}\mathbf{m}\|^2 + \alpha \sum_{k=1}^{N_m} \frac{m_k^2}{m_k^2 + \beta^2} = \min. \tag{10.29}$$

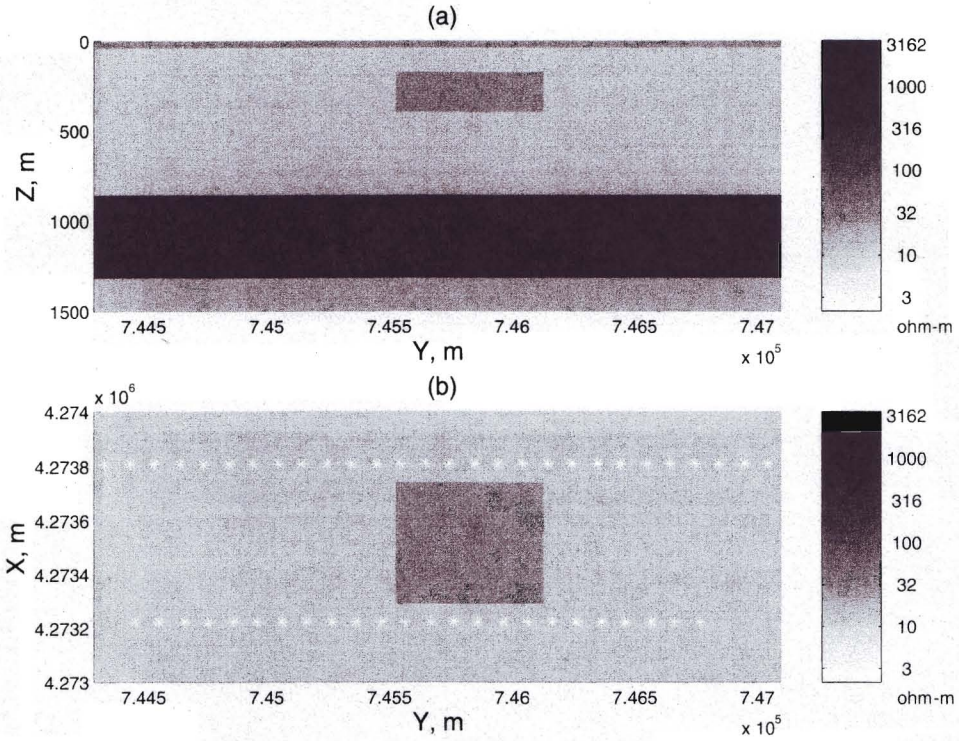

Figure 7. Model with the body inside the conductive layer. (a) Cross-section. (b) Plan view.

Note that problem (10.29) can be expressed as bilinear, using (10.27):

$$\|\mathbf{d} - \widehat{\mathbf{G}}_{\mathbf{j}} \operatorname{diag}(\mathbf{e}_{\mathbf{t}})\widehat{\mathbf{S}}_{\mathbf{e}}\mathbf{m}\|^2 + \alpha \sum_{k=1}^{N_m} \frac{m_k^2}{m_k^2 + \beta^2} = \min, \tag{10.30}$$

$$\mathbf{e}_{\mathrm{t}} = (\widehat{\mathbf{I}} - \widehat{\mathbf{G}} \operatorname{diag}(\widehat{\mathbf{S}}_e \mathbf{m}))^{-1} \mathbf{e}_{\mathrm{n}}. \tag{10.31}$$

The main problem with the IE method is that, for general 3-D cases, matrix $\widehat{\mathbf{G}}$ in Equation (10.31) is full and may be very large. Assume that the anomalous domain D is a rectangular prism. Each side of the prism is divided into N rectangular prismatic cells. Then the number of cells is $N_c = N^3$. The number of entries in the matrix $\widehat{\mathbf{G}}$ is $(3 \times N_c^3)^2 = 9 \times N^6$. We can see that the number of entries grows as the sixth power of N. This growth is the main limiting factor of the integral equation method. If $N = 5$ the problem is small and readily solvable. Yet, for $N = 10$ the size of the problem becomes very large.

The use of focusing inversion greatly reduces the size of the problem. Numerical solution of (10.30) and (10.31) follows conventional bilinear approaches. First we solve (10.30) for $\mathbf{m}$, using some approximation to multiplier $\mathbf{e}_{\mathrm{t}}$. Note that if $\mathbf{e}_{\mathrm{t}}$ is known, problem (10.29) becomes purely linear.

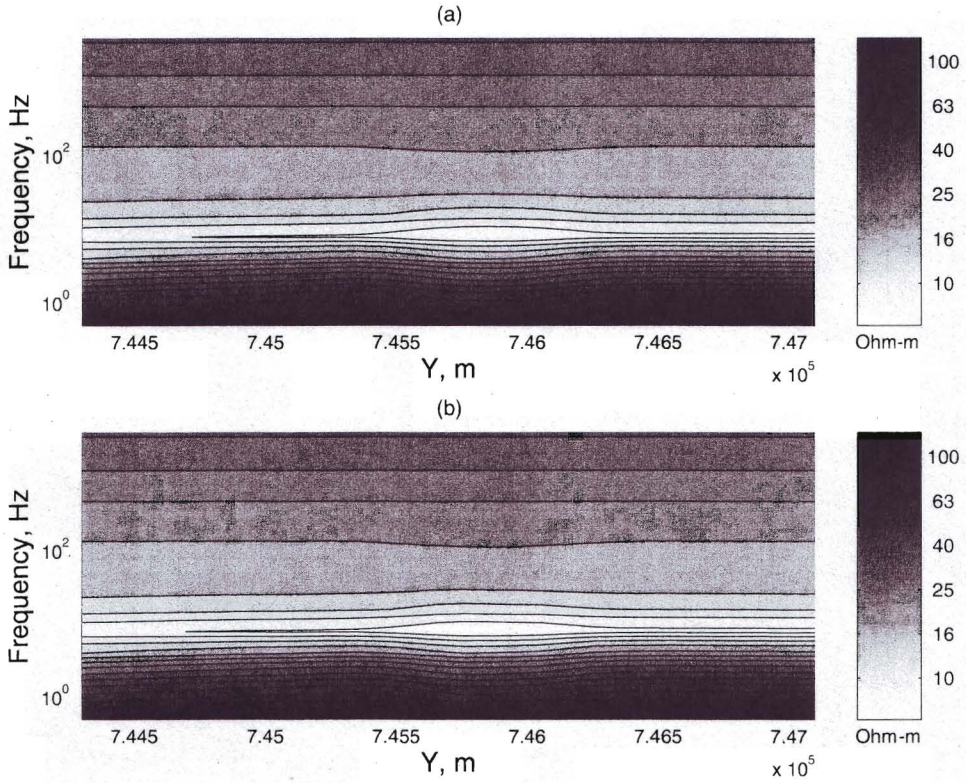

Figure 8. Original apparent resistivity data simulated by SYSEM (case a) and the data predicted from the inversion (case b) for the model with the body inside the conductive layer.

All subsequent iterations deal with a greatly reduced problem. For example, on the second bilinear iteration we use the value of $\mathbf{m}$ to update $\mathbf{e}_t$ using (10.31). But $\mathbf{m}$ has already become sparse, after solving (10.30).

It is very important to find a good initial approximation to the unknown multiplier $\mathbf{e}_t$. The choice of the initial guess determines the course of the inversion. To derive the initial approximation to the multiplier $\mathbf{e}_t$, we use the first iteration of Jacoby's method. According to Jacoby's method, off-diagonal terms (10.13) are neglected:

$$\mathbf{e}_t = \left[\mathrm{diag}(\widehat{\mathbf{I}} - \widehat{\mathbf{G}}\mathbf{S})\right]^{-1} \mathbf{e}_n. \tag{10.32}$$

If we consider an anomalous domain consisting of one cell, (10.32) gives the exact solution. It will also be exact if we consider multiple cells located far away from each other. Physically, this means that the method provides the solution with no electromagnetic interaction between the currents in different cells.

Note also that this approach implicitly assumes the secondary field to be proportional to the primary field. This assumption is similar to the idea of quasi-linear approximation (Zhdanov and Fang, 1996a,b).

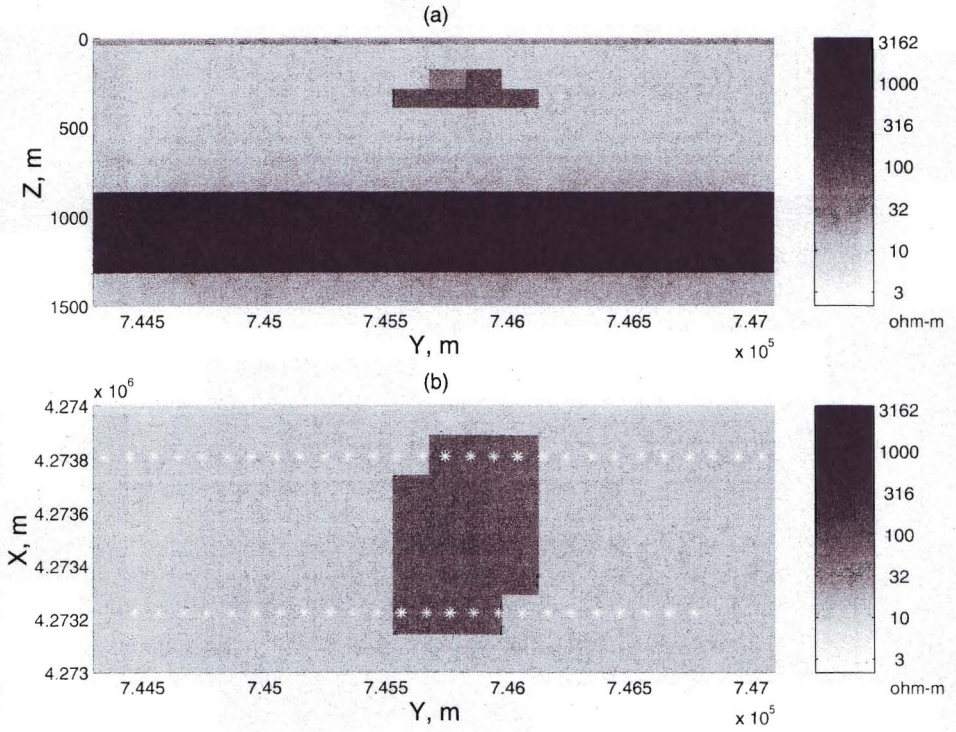

Figure 9. Result of inversion for the model with the body inside the conductive layer. (a) Cross-section. (b) Plan view.

5. BILINEAR CORRECTIONS WITH A MODIFIED GREEN'S OPERATOR

The purpose of subsequent steps in the inversion problem is the following: the nonlinear cross-influence of cells leads to changes in the shape and size of the anomalous bodies but does not change the location of the bodies.

An important question is the convergence of the algorithm. To ensure convergence, we have to modify the Green's matrix $\widehat{\mathbf{G}}$. In other words, we have to condition Equation (10.11) with the conditioners (diagonal matrices) $\widehat{\mathbf{K}}$, $\widehat{\mathbf{A}}$ and $\widehat{\mathbf{B}}$:

$$\mathbf{e}_a = \widehat{\mathbf{G}}\widehat{\mathbf{S}}(\mathbf{e}_a + \mathbf{e}_n); \quad \widehat{\mathbf{K}} = \widehat{\mathbf{A}} - \widehat{\mathbf{B}}; \quad 2\widehat{\mathbf{K}}\widehat{\mathbf{B}} = \widehat{\mathbf{S}}, \tag{10.33}$$

which yields

$$(\widehat{\mathbf{A}} - \widehat{\mathbf{B}})\mathbf{e}_a = \widehat{\mathbf{K}}\widehat{\mathbf{G}}(2\widehat{\mathbf{K}}\widehat{\mathbf{B}})(\mathbf{e}_a + \mathbf{e}_n), \tag{10.34}$$

which we modify further:

$$\widehat{\mathbf{A}}\mathbf{e}_a + \widehat{\mathbf{B}}\mathbf{e}_n = \widehat{\mathbf{K}}\widehat{\mathbf{G}}(2\widehat{\mathbf{K}}\widehat{\mathbf{B}})(\mathbf{e}_a + \mathbf{e}_n) + \widehat{\mathbf{B}}\mathbf{e}_a + \widehat{\mathbf{B}}\mathbf{e}_n. \tag{10.35}$$

Introducing the modified Green's operator $\widehat{\mathbf{G}}_m$ (Zhdanov and Fang, 1997)

$$\widehat{\mathbf{G}}_m(\mathbf{x}) = \widehat{\mathbf{K}}\widehat{\mathbf{G}}2\widehat{\mathbf{K}}(\mathbf{x}) + \mathbf{x}, \tag{10.36}$$

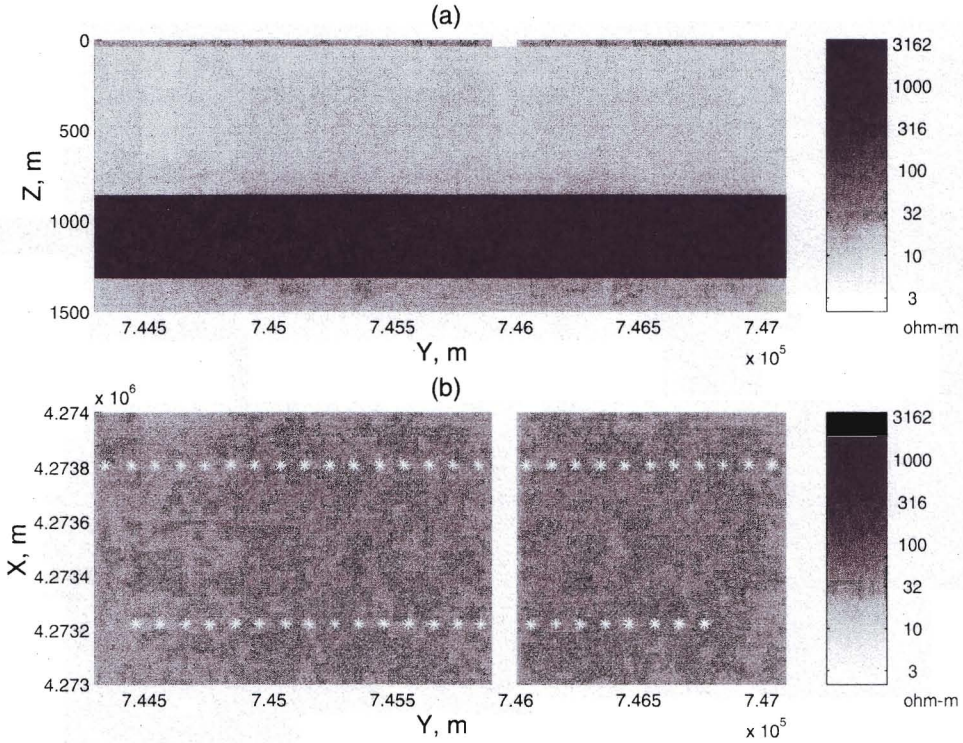

Figure 10. Model with a near-surface local conductive body. (a) Cross-section. (b) Plan view. Stars show the observation points located on the surface. The body is located near coordinate $Y = 746000$ m.

we have

$$\widehat{\mathbf{A}}\mathbf{e}_{\mathrm{a}} + \widehat{\mathbf{B}}\mathbf{e}_{\mathrm{n}} = \widehat{\mathbf{G}}_m(\widehat{\mathbf{B}}\mathbf{e}_{\mathrm{a}} + \widehat{\mathbf{B}}\mathbf{e}_{\mathrm{n}}). \tag{10.37}$$

It has been proven (Zhdanov and Fang, 1997) that the modified operator $\widehat{\mathbf{G}}_m$ has the contraction property

$$\|\widehat{\mathbf{G}}_m(\mathbf{x})\| < \|\mathbf{x}\|, \tag{10.38}$$

provided that the conditioners $\widehat{\mathbf{A}}$ and $\widehat{\mathbf{B}}$ are connected to normal $\widehat{\mathbf{S}}_{\mathrm{n}}$ and anomalous conductivity distribution $\widehat{\mathbf{S}}$ via the relationships

$$\widehat{\mathbf{A}} = \widehat{\mathbf{S}}_{\mathrm{n}}^{-1/2}(2\widehat{\mathbf{S}}_{\mathrm{n}} + \widehat{\mathbf{S}})/2, \quad \widehat{\mathbf{B}} = \widehat{\mathbf{S}}_{\mathrm{n}}^{-1/2}\widehat{\mathbf{S}}/2. \tag{10.39}$$

Property (10.38) ensures convergence of the algorithm. Therefore, instead of (10.31) we iterate Equation (10.37) to solve for $\mathbf{e}_{\mathrm{a}}$, from which we obtain the unknown multiplier $\mathbf{e}_{\mathrm{t}}$, using Equation (10.10).

6. TESTS ON MODELS

We have applied 3-D focusing inversion to synthetic CSAMT data. We consider two sets of models.

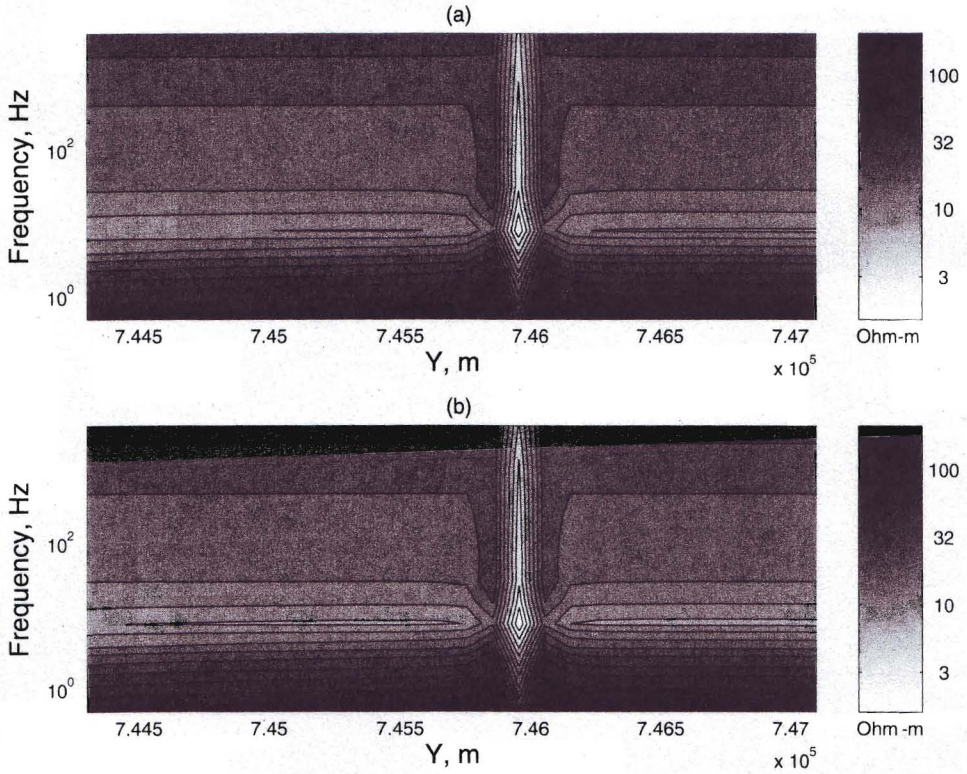

Figure 11. Original data simulated by SYSEM (case a) and the data predicted from the inversion (case b) for the model with the local body near the surface.

The first model contains two conductive (1 Ohm m) bodies embedded in a 20-Ohm m background, with their centers located at a depth of 600 m, 300 m apart. For the full 3-D interpretation we have simulated the data on three parallel profiles (Figure 1, case a). The horizontal electric bipole transmitter AB was located 8 km away from the central profile. Panel b in this figure depicts the true model.

Figure 2 shows the inversion results. Smooth inversion (case a) cannot resolve the bodies. The focusing inversion (case b) resolves the bodies well. Both models in Figure 2 fit the data with the same accuracy of 1.5% (r.m.s. average).

Note that focusing inversion makes strong assumption about compactness of material property distribution. That is why the apparent resolution is so good.

The other model contains a resistive (2600 Ohm m) layer covered by a conductive (10 Ohm m) layer of 900 m in thickness. This model uses the survey geometry which is shown in Figure 3. The same figure shows the discretization for the inverse problem, where the top of the lower half-space is filled with cells increasing in size with depth. We calculate apparent resistivity at 14 frequencies ranging from 0.5 Hz to 4096 Hz, on two profiles located as shown in Figure 3. These parameters are based on the real exploration problem described in the last subsection of this paper.

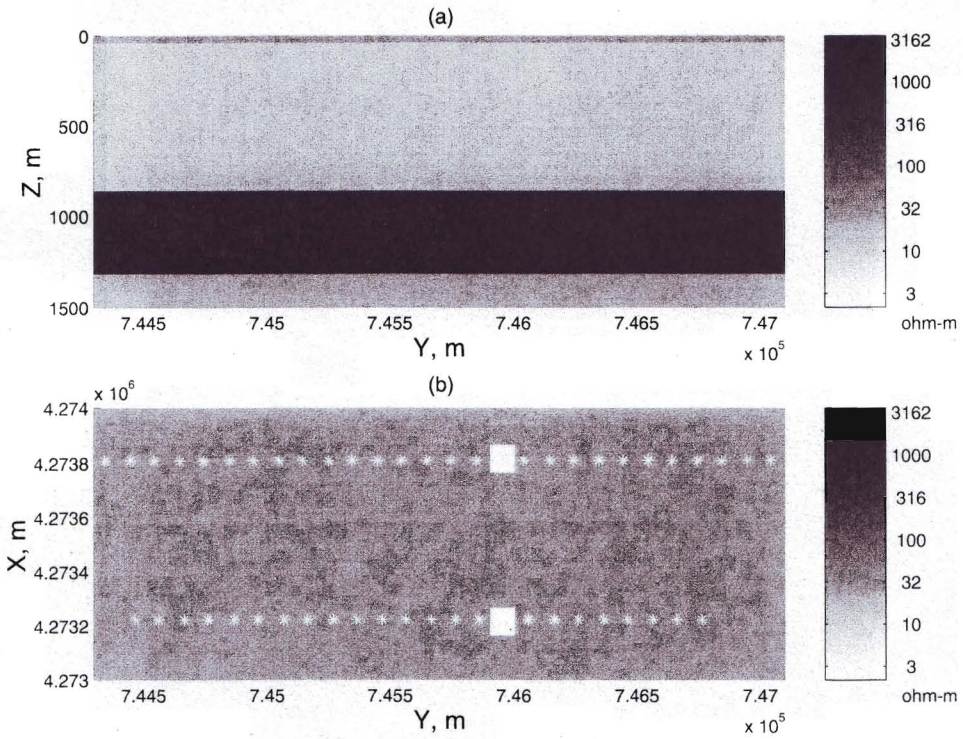

Figure 12. The inversion result for a local, near-surface body. (a) Cross-section. (b) Plan view. Inversion resolves the bodies below the observation profiles but does not resolve the bodies' strike extent away from the profiles.

The problem is to find the topography of the upper boundary of a layer. For example, an anticline structure can be viewed as a departure from the horizontally layered background. It can be modeled as an anomalous resistive body located atop the layer, like the one shown in Figure 4. Figure 5, case a, shows the data (apparent resistivity) computed for this model by the SYSEM full IE forward modeling code (Xiong, 1992). Case b in Figure 5 shows the data predicted from the inversion. The result of inversion for this model is shown in Figure 6.

In a real exploration problem, however, anomalies in the upper layers often overshadow the deeper structures. In the MT and CSAMT method this effect is called 'static shift'. The last two models illustrate this point. Let us consider the model where the observation system and background are the same, but the conductive layer contains a resistive inclusion in it, as shown in Figure 7. Figure 8 shows observed (case a) and predicted apparent resistivity data (case b) for this model. Figure 9 shows the result of inversion for this model. Another model consists of a local near-surface conductive body. This model is depicted in Figure 10. The response from this model is shown in Figure 11. Figure 12 shows the result of inversion for this body. As we can see, inversion can compensate for the static shift effects, but cannot resolve a near-surface structure located between the profile.

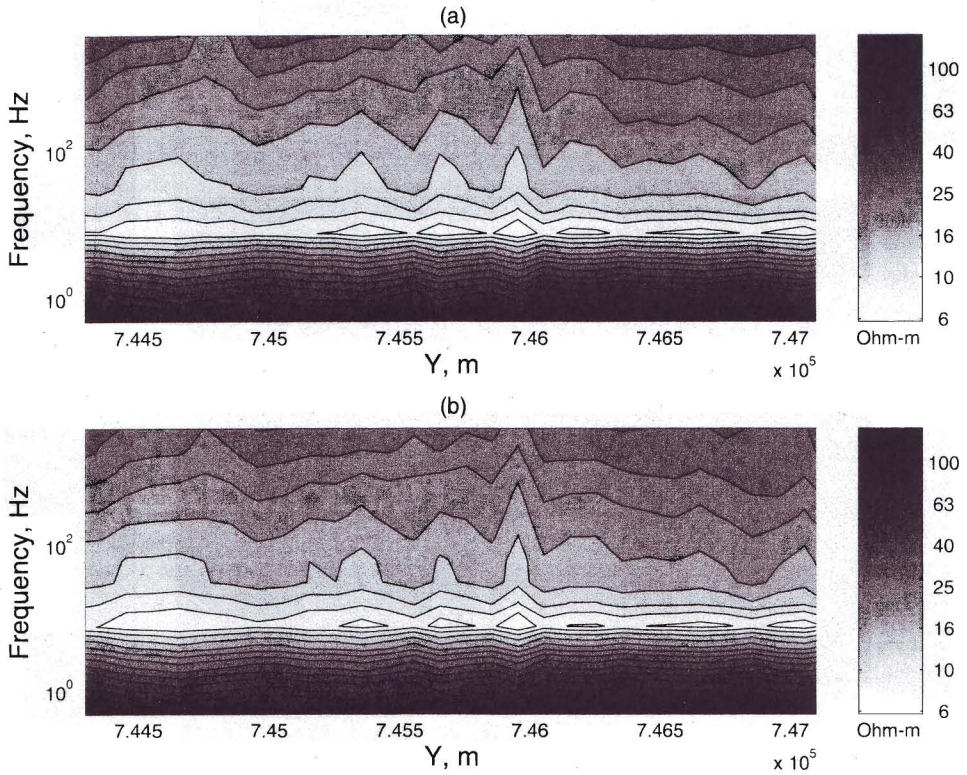

Figure 13. Apparent resistivity on the first profile (a) observed, (b) predicted from 3-D inversion.

7. INVERSION OF REAL DATA

We applied the developed method to the inversion of real 3-D CSAMT data collected in Hamlin Valley for oil exploration. Detailed description of this example is given in Portniaguine (1999).

The observation system is similar to that in Figure 3. We have applied 3-D inversion to the two profiles simultaneously. For the full 3-D interpretation we used the original data uncompensated for static shift (Figure 13). The compensation for static shift is left to the inversion. Panel a in this figure depicts the observed data (apparent resistivity). Panel b depicts the data predicted from inversion. The misfit (global r.m.s. error) was 1%.

Figure 14 shows the inversion results. The stars in panel b are superimposed on the top of the resistive layer. They are picked from the seismic section at the same location and correlated with the Devonian layer. This figure depicts two interesting features. First, we can see that 3-D inversion accurately predicts a down-dropped block in the Devonian. Second, we can see the uplifted part of the fault. Thus, with the 3-D CSAMT inversion, we were able to reach the same conclusions as from the seismic data.

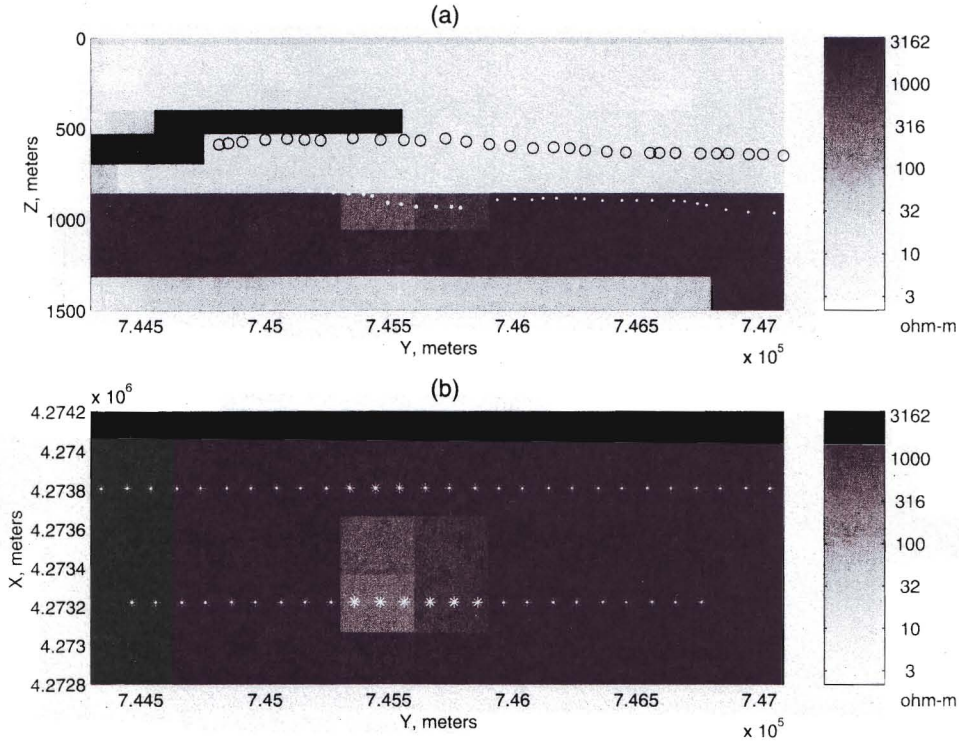

Figure 14. (a) Cross-section of the resulting resistivity model along the first profile. (b) Horizontal slice of the resulting model taken at 800 m depth.

8. CONCLUSION

We have developed a new algorithm of 3-D CSAMT data inversion based on integral equation forward modeling and regularized inversion. This algorithm combines the ideas of the iterative Born method and focusing imaging.

For inversion, we converted the CSAMT data to log-anomalous apparent resistivity, which was linearly connected to anomalous fields. Such a conversion simplifies the inversion algorithm and is convenient to use.

The results of our work demonstrated that the combination of iterative Born method and focusing regularized inversion resulted in a new effective method of CSAMT data interpretation over 3-D geoelectrical structures.

ACKNOWLEDGEMENTS

The authors acknowledge the support of the University of Utah Consortium for Electromagnetic Modeling and Inversion (CEMI), which includes Advanced Power Technologies Inc., AGIP, Baker Atlas Logging Services, BHP Minerals, ExxonMobil Upstream

Research Company, Geological Survey of Japan, INCO Exploration, Japan National Oil Corporation, MINDECO, Naval Research Laboratory, Rio Tinto–Kennecott, 3JTech Corporation, and Zonge Engineering. We thank Kriac Energy, Inc. for providing Hamlin Valley data.

REFERENCES

Cagniard, L., 1953. Basic theory of the Magneto-Telluric method of geophysical prospecting. Geophysics, 18, 605–645.

Chew, W.C., 1990. Waves and Fields in Inhomogeneous Media. Van Nostrand Reinhold, New York.

Habashi, T.M., Groom, R.W. and Spies, B.R., 1993. Beyond the Born and Rytov approximations: a non-linear approach to electromagnetic scattering. J. Geophys. Res., 98, 1759–1775.

Hohmann, G.W., 1975. Three-dimensional induced polarization and EM modeling. Geophysics, 40, 309–324.

Portniaguine, O., 1999. Image Focusing and Data Compression in the Solution of Geophysical Inverse Problems. Ph.D. dissertation, University of Utah.

Portniaguine, O. and Zhdanov, M.S., 1998. Focusing geophysical inversion images. SEG 68 Annual Meeting in New Orleans, Sep. 13–18, Expanded abstracts, pp. 465–468.

Portniaguine, O. and Zhdanov, M.S., 1999. Focusing geophysical inversion images. Geophysics, 64, 874–887.

Rudin, L.I., Osher, S. and Fatemi, E., 1992. Nonlinear total variation based noise removal algorithms. Physica D, 60, 259–268.

Tikhonov, A.N., 1950. On the determination of electrical characteristics of deep layers of the Earth's crust (in Russian). Dokl. Akad. Nauk SSSR, 73, 295–297.

Tikhonov, A.N. and Arsenin, V.Y., 1977. Solution of Ill-Posed Problems. V.H. Winston and Sons, Washington, DC, 223 pp.

Vogel, C.R. and Oman, M.E., 1998. A fast, robust total-variation based reconstruction of noisy, blurred images. IEEE Trans. Image Process., 7, 813–824.

Weidelt, P., 1975. EM induction in three-dimensional structures. Geophysics, 41, 85–109.

Xiong, Z., 1992. EM modeling of three-dimensional structures by the method of system iteration using integral equations. Geophysics, 57, 1556–1561.

Zhdanov, M.S., 1993. Tutorial: regularization in inversion theory. Colorado School of Mines, Golden, CO, 47 pp.

Zhdanov, M.S. and Fang, S., 1996a. Quasi-linear approximation in 3-D EM modeling. Geophysics, 61(N 3), 646–665.

Zhdanov, M.S. and Fang, S., 1996b. 3-D quasi linear electromagnetic inversion. Radio Sci., 31(4), 741–754.

Zhdanov, M.S. and Fang, S., 1997. Quasi-linear series in three-dimensional electromagnetic modeling. Radio Sci., 32, 2167–2188.

Zhdanov, M.S. and Keller, G.V., 1994. The Geoelectrical Methods in Geophysical Exploration. Elsevier, Amsterdam, 873 pp.

Zhdanov, M.S., Dmitriev, V.I., Fang, S. and Hursan, G., 2000. Quasi-analytical approximation and series in electromagnetic modeling. Geophysics, 65, 1746–1757.